JAMES F. CARBARY, GLEN H. FOUNTAIN, JOHN S. HANSEN, DENNIS E. FORT, and CHING-I. MENG

ULTRAVIOLET- AND VISIBLE-WAVELENGTH MEASUREMENTS FROM LOW EARTH ORBIT

From the vantage of low Earth orbit, modern electro-optical instruments can observe characteristic atmospheric features. A recent Department of Defense mission scanned the Earth limb under fully sunlit, partially moonlit, and near-terminator conditions and measured atmospheric emissions in the 130- to 725-nm spectral regime. Spectrographic and imaging instruments identified atmospheric emissions from species such as atomic oxygen, nitric oxide, and sodium; pitching maneuvers of the spacecraft platform allowed the altitudinal profiles of these emissions to be determined. Additionally, the instruments observed the Moon and several stars. The measurements calibrated the instruments' responses to distinct points and edges and revealed the smearing of three to five pixels in the definition of an edge.

INTRODUCTION

Emissions at ultraviolet and visible wavelengths have been important investigative tools of atmospheric science since the beginning of the space age. Early investigations typically used a rocket to carry a photometer or spectrometer briefly above the lower atmosphere to determine the altitudinal profiles of airglow and auroral emissions.[1-4] Satellites such as OGO-4, ISIS-2, and the Nimbus series provided orbital platforms that extended such radiometric measurements for longer times.[5-9] Antarctic ozone depletion has stimulated interest in atmospheric ultraviolet emissions because their spectra can be used to measure ozone abundance from low Earth orbit.[10-12] Photometric imagers on the DE-1 satellite used ultraviolet and visible radiation to image the global state of the upper atmosphere.[13,14] In the mid-1980s, the space shuttle provided a platform for several detailed spectrographic studies of the airglow in the ultraviolet and visible regimes.[15,16] Investigators at APL have concentrated on ultraviolet wavelengths below 250 nm to make the first images of the aurora in sunlight.[17-19]

As part of a mission to measure background radiation from low Earth orbit, APL recently developed an instrument that observes at ultraviolet and visible wavelengths. The instrument, designated U2, combines both imaging and spectrographic systems. Such a combination of systems in a single experimental package is virtually unknown in the history of satellite measurements. The U2 combination permits simultaneous measurement of the ultraviolet and visible scenes and their full spectral characteristics.

The spacecraft carrying the U2 instrument was launched during the winter in the Northern Hemisphere. It had an elliptical orbit of 222 by 343 km, with an inclination of 28°. During the mission, the U2 instrument observed four principal background scenes: the Earth limb, the Moon, space without bright stars in the field of view, and space with a single bright star in the field of view. Within the Earth-limb category, U2 made five complete altitude scans across the noon, midnight, dawn, and dusk horizons. The single-star observations allowed the instruments to look at stars of two spectral types (B and F), which served as calibration sources. Observations of the stars and the Moon allowed an unambiguous determination of the response of the instruments to sharp point and edge sources. Table 1 summarizes the several backgrounds sampled by the U2 instrument.

INSTRUMENT DESCRIPTION

The U2 instrument consisted of two imagers and four spectrographs that were designed to measure optical emissions in the 130- to 725-nm wavelength range. Figure 1 is a block diagram of the instrument. The spacecraft provided both power and operational commands to the device. An inertial guidance system pointed the instruments to within 1° of the desired observational direction. Because on-board tape recorders stored the data, the U2 could operate for approximately 4 h at a data rate of 1.05 Mb/s before transmission to the ground. That data rate allowed the instrument to generate an image every 1.6 s from one of the two imagers and a spectrum every 0.2 s from each of the four spectrographs.

Both the imagers and the spectrographs viewed forward along the longitudinal axis of the spacecraft platform. The imagers had relatively large fields of view, fixed in the forward-looking direction. The spectrographs had much smaller fields of view and used a gimballed mirror device to point in their look directions. The gimbal mirrors could accept pointing information from the on-board guidance system, execute preprogrammed scan patterns, or point straight ahead along the spacecraft axis. The spectrographs executed a cruciform scan pattern during the star observations but were programmed to look straight ahead during the other observations presented here.

Sunshades were attached to both the imagers and the spectrographs to reduce off-axis light scattered into the

Table 1—Summary of background targets.

Common Name	*Astronomical Name*	*Spectral Class*	*Visual Magnitude*	*Observational Range*
Earth limb	Earth	(Atmospheric and solar emissions)	—	2050 km
Moon	Luna	(Solar emissions)	−12.5*	3.8×10^5 km
Canopus	Alpha Carina	F0 Ib	−0.75	110 light-years
Mimosa	Beta Crucis	B0.5 III	1.26	490 light-years
Procyon	Alpha Canis Major	F5 IV-V	0.37	11 light-years

*The value given is the apparent magnitude.

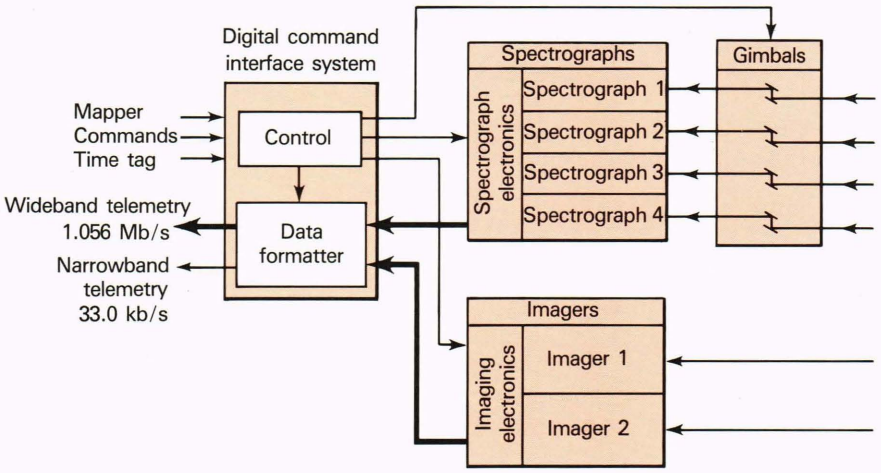

Figure 1—Block diagram of the U2 instrument. The spectrographs and the imagers occupy the right-hand side of the diagram, and the power and electronics occupy the left-hand side. Communication and data flow between the detectors and the spacecraft were handled by the digital command interface system.

telescopes from the Sun and the Earth. The imager shades rejected light at cone angles exceeding 32.5°, and the spectrograph shades rejected light at angles greater than 33.5° to 35.0°, depending on the azimuth angle of the incident light. The sunshades reduced light levels by 9 to 10 orders of magnitude for angles greater than the rejection angles. Figure 2 shows the U2 instrument, complete with sunshades, as it appeared before mounting on the spacecraft.

IMAGERS

Each of the two imagers had a 51-mm reflecting telescope, a six-position filter wheel, an image-intensified charge-coupled device (CCD) camera, and electronics to process the image. Imager 1 operated at ultraviolet wavelengths, and imager 2 operated at visible wavelengths. The choice of intensifier photocathode determined the wavelength regime of each imager. Table 2 summarizes the operational parameters of the imagers.

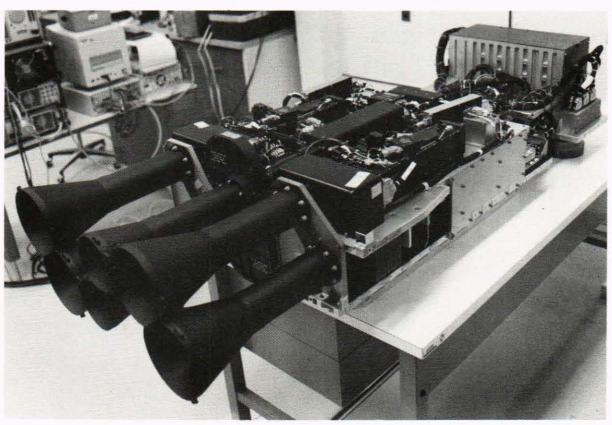

Figure 2—Photograph of the U2 instrument before mounting on the spacecraft. The black hornlike structures are the sunshades. The detectors occupy space both above and below the middle deck of the pallet. The electronics sits at the rear of the pallet.

Table 2—Imager operational parameters.

Imager 1 bandpasses*	
1. Clear neutral density ($\times 10^0$)	130–290 nm
2. 135-nm bandpass	130–155 nm
3. 165-nm bandpass	155–186 nm
4. 220-nm bandpass	212–237 nm
5. 270-nm bandpass	260–286 nm
6. Clear neutral density ($\times 10^{-1}$)	130–290 nm
Imager 2 bandpasses*	
1. Clear neutral density ($\times 10^0$)	320–725 nm
2. 300-nm bandpass	290–311 nm
3. 340-nm bandpass	331–353 nm
4. 560-nm bandpass	550–573 nm
5. 630-nm bandpass	622–642 nm
6. Clear neutral density ($\times 10^{-2}$)	320–725 nm
Nominal field of view	1.9° × 2.1°
Resolution per pixel	200 μrad
Sensitivity	1000 Rayleighs†
Intrascene dynamic range	256 (8 bits)
Interscene dynamic range	10^8
Nominal scene image rate	0.3 images/s
Nominal aperture area	6.8 cm^2

*A full width at half maximum bandpass measurement was taken.
†1 Rayleigh = $4\pi/10^6$ × source radiance in photons/cm^2 s sr.

The imager electro-optics consisted of three major units: the imaging head (optical train, intensifier, and CCD), the camera electronics, and the control and digitization electronics. Filters placed in front of each telescope could be rotated into the optical path by using a Geneva wheel mechanism. Each imager telescope employed a Cassegrainian design with two spherical mirrors and a 478-mm focal length. With the photocathode located in the image plane of the telescope, each image intensifier provided gain for scenes at low light levels and converted all input light into green light. The green-light intensifier output was coupled to a CCD by a fiber-optic reducer. The reducer mapped the intensified image (25-mm diagonal) onto the rectangular area of the CCD (14.7-mm diagonal), and the camera electronics converted the CCD output into a standard video output, which was then converted by digitization electronics into a 384 by 488 pixel array. The pixel array was stored in a video memory before transfer to the tape recorder. An automatic gain control circuit monitored the pixel intensities and adjusted the imager gain so that nearly all the pixel intensities stayed within 15% to 80% of full scale. The gain intensity was adjusted either by changing the intensifier voltage levels or by time gating the accumulation time.

SPECTROGRAPHS

Each of the four spectrographs consisted of a telescope, a 125-mm Ebert mount mirror and grating arrangement, an intensified linear array detector, and processing electronics. As with the imagers, the wavelength bands covered by each spectrograph were determined by the appropriate selection of photocathode material and by a bandpass filter located behind the telescope image plane. The spectrographs' small fields of view (0.5°) represented a compromise between improved spectral resolution and reasonable pointing requirements. Table 3 summarizes the operational parameters of the spectrographs.

The spectrograph optics consisted of two gimbal mirrors that rotated about orthogonal axes, a telescope, and a filter wheel located immediately in front of the telescope focal plane (the spectrograph entrance aperture). The telescope had an off-axis parabolic mirror with a focal length of 23 cm and a nominal collection area of 18 cm^2.

The filter wheel provided partial control of the spectrograph sensitivity and spectral resolution. A clear, 2.0-mm aperture at the focal plane allowed each spectrograph to operate with a nominal 0.5° (half-angle) circular field of view and a spectral resolution worse than that given in Table 3 by about a factor of 6. A small, 0.5-mm aperture in front of the focal plane reduced the field of view and provided the maximum spectral resolution (Table 3 value). The improved spectral resolution was used for Earth-limb observations. A 2.0-mm aperture with an attenuating neutral density filter reduced the intensity by a factor of 100. The final position of the filter wheel closed the input aperture to permit instrument noise measurements.

The spectrograph optics imaged the input aperture onto the image intensifier photocathode. The image was dispersed in wavelength along a 25-mm line on the photocathode. Each spectrograph's grating had a dispersion constant that tailored it for the desired wavelength coverage. In response to incident photons, the intensifier output generated green light, which was converted into an electrical charge by the linear array detector. A 128-pixel spectrum was read out of the linear array every millisecond. To reduce the data rate to a manageable size, 200 of these spectra were summed and transmitted as 128 16-bit words every 0.2 s.

The intrinsic dynamic range of each spectrograph was limited mainly by the 16-bit word size and also by the number of photons that could be collected in one pixel in 1 ms without saturating the detector electronics. Therefore, the intrascene dynamic range was limited to 2^{16} (Table 3). The brightest scene observed was more than 2^{16} brighter than the darkest scene observed, so the spectrographs had two additional ways to improve sensitivity. First, an automatic gain control monitored the spectral amplitude and used an intensifier gating mechanism to vary the sensitivity in steps that increased by factors of 2 from 0.4% to 100%. Second, the 0.01 neutral density filter could be inserted by command. In combination, these mechanisms extended the interscene dynamic range of each spectrograph to 10^8.

CALIBRATIONS

Because of the abbreviated schedule of the mission, the U2 instruments could not undergo the usual cycle

Table 3—Spectrograph operational parameters.

Spectrograph number	1	2	3	4
Wavelength (nm)	122–229	176–334	301–454	447–710
Spectral resolution (nm)	<1.6	<2.4	<2.4	<4.0
Minimum flux (photons/cm^2 s)	341	11	16	37
Nominal field of view	0.5° circular			
Nominal field of regard	6° circular			
Intrascene dynamic range	2^{16}			
Interscene dynamic range	10^8			

of calibrations and recalibrations that usually attends the development of research-caliber optical instruments. The spectrographs and the imagers did undergo both vacuum-chamber calibrations (at the Air Force Geophysics Laboratory) and open-air optical bench calibrations (at APL). The spectrograph calibrations included field of view, wavelength of bins, efficiency as a function of wavelength, dynamic range of the automatic gain controls, and instrumental background noise. The imagers were calibrated for field of view, uniformity across the field of view, efficiency, dynamic range of the automatic gain controls, and instrumental background noise at various temperatures. The imager filter transmissivities were calibrated separately.

During flight, calibrations continued with observations of the Moon and several stars with known spectra. Adjustments to the spectrograph calibration were necessary to ensure continuity of the spectrum across the four spectral regions sampled by U2 and to bring the observed spectrum into closer agreement with the known stellar spectra. The calibration effort continues. Presently, spectrographic measurements may contain errors in absolute intensities as great as factors of 3 to 4, especially near the ends of spectral bandwidths. The following analysis has omitted data from those regions whenever possible.

The U2 imagers apparently suffered some degradation in the uniformity of the CCD photocathode. Several small spots appeared in the ultraviolet imager, and a larger blemish appeared in one corner of the visible imager. The ground calibrations did not reveal such blemishes, which must have occurred before the initial observations. Fortunately, the blemishes did not seriously affect the overall quality of the images. Preliminary comparisons of the imager data with known stellar radiation indicate that the ultraviolet imager has an error of about 30% in measuring the absolute photometry of a point source, and the visible imager has a somewhat greater error. As discussed in the following section, the imagers may have also suffered some optical defocusing.

EARTH-LIMB OBSERVATIONS

The spacecraft executed a series of pitch maneuvers that allowed the instrument to scan up and down across the Earth limb. The U2 made five scans each of the noon, midnight, dawn, and dusk limbs of the Earth. During the observations, the vehicle platform pointed approximately toward the northern horizon and pitched from orbit-normal elevations near −5° (zenith angle = 95°) to elevations as low as −21° (an elevation of 0° corresponds to viewing tangent to the orbit). Such elevations allowed the instruments to effectively sample tangent altitudes from 250 km above to 150 km below the hard-Earth horizon. In effect, both the imagers and the spectrographs obtained continuous altitude profiles of the limb emissions. Furthermore, the orbital motion of the spacecraft allowed the instrument to sample in local time; this feature added a third dimension to the measurements. Local time variations become especially important across the terminator in the twilight environment.

Noon Limb

The Earth's noon limb presented the brightest background observed by the U2 instrument and actually caused spectrographs 3 and 4 to saturate at elevations below the horizon (i.e., when viewing the hard-Earth background). These units recovered with no ill effects when the vehicle pointed above the horizon into less radiant regimes.

Figure 3 shows the noon limb horizon as observed by the U2 visible imager (320 to 725 nm). The imager field of view corresponds to a frame size of 85 by 65 km at the tangent range of the horizon (≈2050 km). The frame shows a tilted view of the Earth horizon, with the solid Earth located in the lower left-hand corner of the frame and space located in the upper right-hand corner. The hard-Earth horizon runs diagonally from the upper left to the lower right. Contours of yellow, green, and blue show layers in the lower atmosphere. In the lower left-hand corner, faint red streaks on yellow indicate cloud

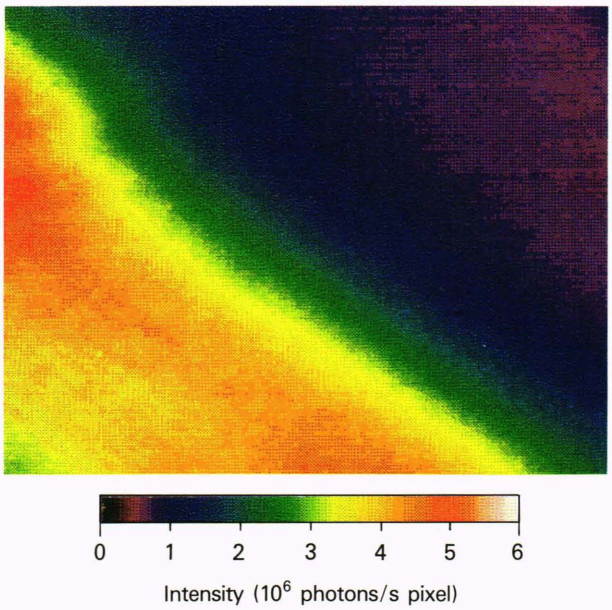

Figure 3—Noon limb viewed by the visible imager (320 to 725 nm). The Earth is at the lower left, space is at the upper right, and the solid-Earth horizon runs along the central diagonal (25.3-km tangent altitude). The frame measures about 85 by 65 km.

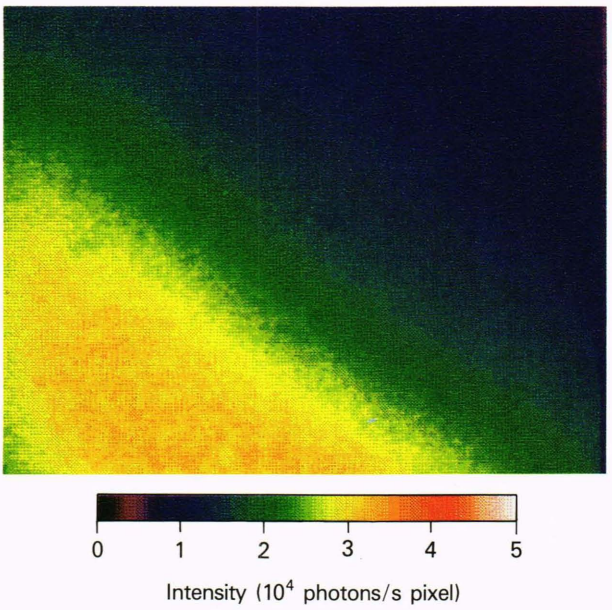

Figure 4—Noon limb viewed by the ultraviolet imager (130 to 290 nm). The frame orientation is the same as in Fig. 3, with the Earth at the lower left. The frame measures about 85 by 65 km and has a 42.5-km tangent altitude.

formations within the troposphere. The colors indicate intensity rather than actual color, and the slight enhancement in the upper left-hand corner represents an uncorrected aberration in the image intensifier rather than an atmospheric bulge.

Figure 4 shows the noon limb horizon as observed by the U2 ultraviolet imager (130 to 290 nm). In this case, the imager sampled space about 40 km above the Earth horizon, and the bright yellow-red band indicates the ultraviolet airglow layer of the noon limb. The ultraviolet airglow appears featureless except for the altitudinal gradations represented by the yellow, green, and blue contours.

The spectrographs revealed a wealth of airglow features in the emissions of the noon limb. Figure 5 shows the entire spectrum of the noon limb at a tangent altitude of about 90 km. Solar backscattered radiation dominates the spectrum at wavelengths longer than 320 nm, although the stronger airglow emissions of oxygen and sodium may be recognized above the solar continuum. One of the most prominent features of the spectrum is the sodium feature at 589 nm. This emission originates in a thin ($\approx$1-km) layer of sodium near an altitude of 90 km. At wavelengths shorter than 320 nm, individual airglow emission features dominate the spectrum. These features include the prominent nitric oxide gamma and, to a lesser extent, delta band emissions between 200 and 300 nm and the oxygen emissions (130.4 and 135.6 nm) below 200 nm.

The continuous operation of the spectrographs at a high data rate allowed unaliased time profiles of the spectra, which can best be displayed in a three-dimensional spectrogram format, as shown in Fig. 6. The two spectrograms show wavelength along the horizontal axis, time

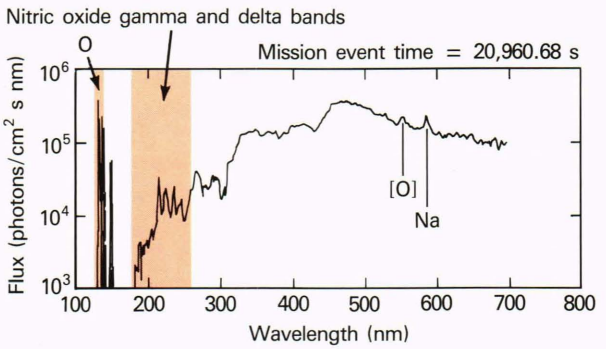

Figure 5—Noon limb spectrum at a tangent altitude of 93.7 km. Various spectral features are marked, including the sodium emission. The spectrum represents a composite formed from data from all four U2 spectrographs.

along the vertical axis, and intensity as a color within the wavelength–time grid. The figure covers complete scans of spectrographs 2 and 4 from below the Earth horizon (at 20,910 s) to the maximum scan altitude (at 20,940 s) to below the Earth horizon (at 20,970 s). The bright regions at the top and bottom of the frame indicate the solar backscatter associated with the Earth horizon, and the vertical "fingers" represent nitric oxide gamma and delta bands, sodium emissions, and oxygen emissions. The decreases in intensity of these fingers toward the centerline of the frame indicate the altitudinal variation of the emissions.

Dusk Limb

The dusk observations permitted the sampling of emissions across the terminator region of the atmosphere.

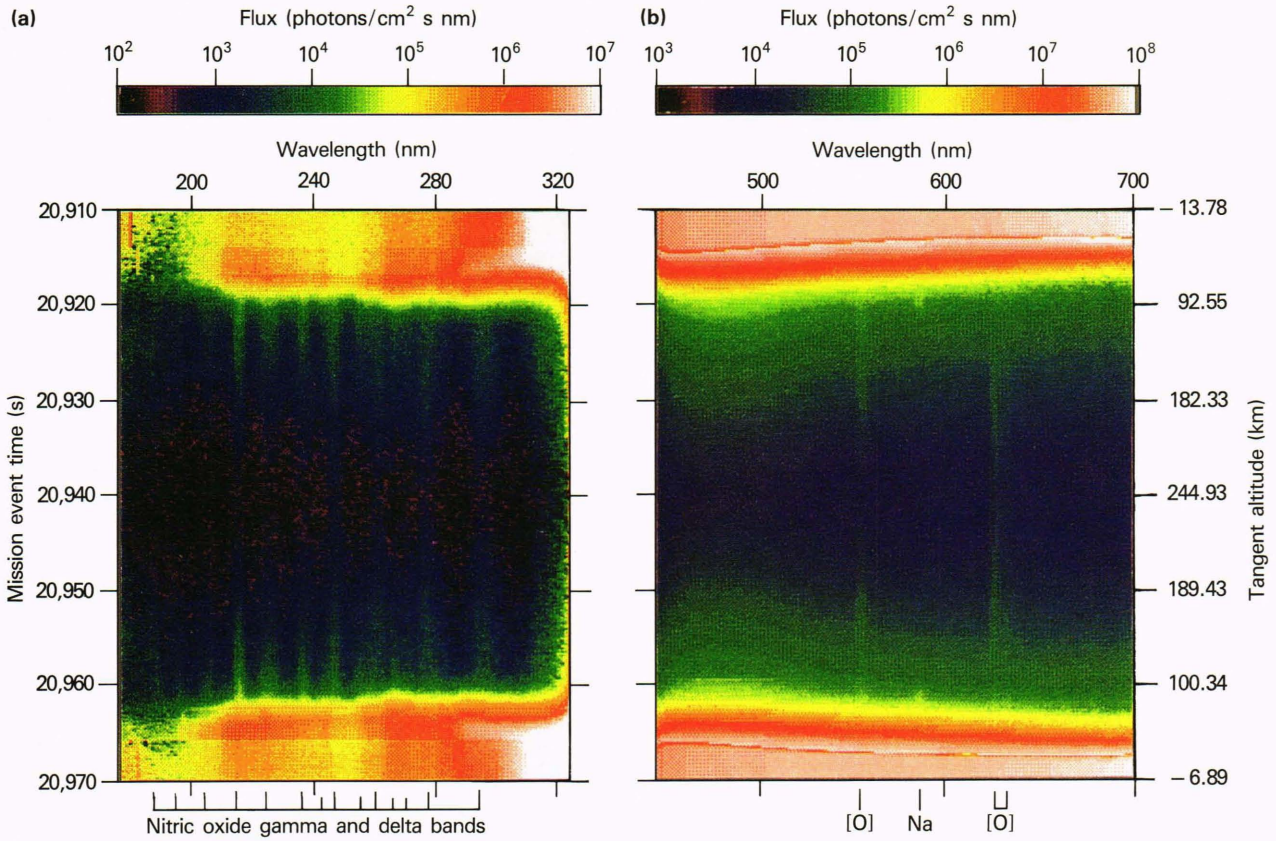

Figure 6—Noon limb spectrogram showing one cycle of a limb scan as observed by (a) spectrograph 2 and (b) spectrograph 4. In this format, the horizontal axis indicates wavelength, the vertical axis represents time, and the color represents intensity in the given wavelength–time bin. The frames are also altitudinal profiles of the spectra.

Generally, dusk emissions are less intense than noon emissions and exhibit stronger local time variations, but both have similar emission features. Figure 7 shows the dusk limb as observed by the U2 visible camera while viewing a tangent altitude near 20 km. The viewing orientation is the same as for the noon limb, with the hard Earth at the lower left-hand corner of the frame and space at the upper right-hand corner. The yellow and green diagonal band across the center of the picture represents a 20-km-thick haze layer along the Earth horizon. The intense red feature near the upper left-hand corner of the frame is an artifact of the imager CCD response and is not an actual atmospheric intensity enhancement. Below the haze layer, one can see rows of clouds in the troposphere. The view looks northward over the Pacific Ocean.

The corresponding ultraviolet scene (not shown) generally exhibits lower photon fluxes and fewer spatial features than the visible scene. As with the noon limb spectrum, the dusk limb spectrum displays emissions from oxygen, nitrogen, and nitric oxide. At the higher altitudes, the forbidden oxygen emissions at 557.7 and 630.0 nm are evident. At the lower altitudes, they disappear, and the backscattered solar continuum emissions begin to predominate.

Figure 8 contrasts the actual altitudinal profiles observed at dusk and noon by spectrograph 2, which ob-

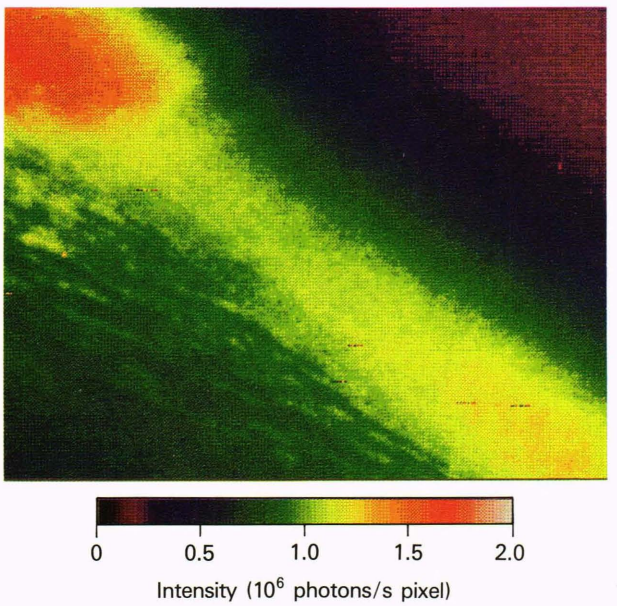

Figure 7—Dusk limb view from the visible imager, in the same format as Fig. 3. The red enhancement in the upper left-hand corner represents an uncorrected blemish on the CCD and not an actual atmospheric feature. The picture shows the solid-Earth horizon (tangent altitude of 20.3 km). Clouds over the Pacific Ocean appear in the lower left-hand portion of the frame.

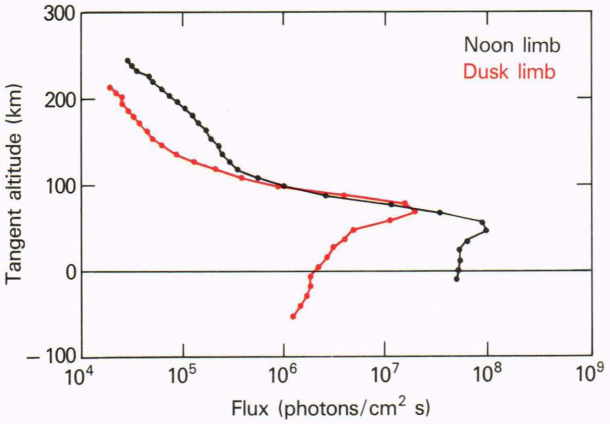

Figure 8—Emission profiles observed by spectrograph 2 of the dusk limb (mission event time = 21,090 to 21,120 s) and noon limb (mission event time = 22,030 to 22,060 s). The fluxes were obtained by summing the data from individual wavelength bins between 177 and 300 nm. A negative tangent altitude indicates the instrument was viewing below the solid-Earth horizon. Each data point represents a 1-s average.

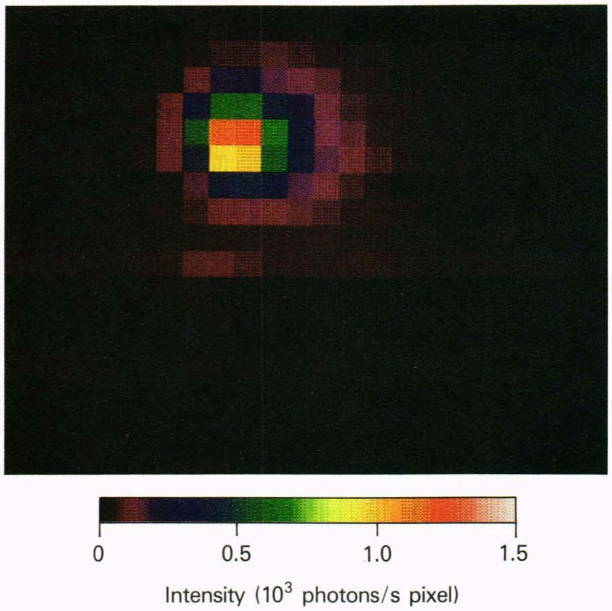

Figure 9—An enlarged image of Mimosa (Beta Crucis) as observed by the visible imager. Ideally, the star would occupy a single pixel, but pixel spreading effects cause the star to have a full width at half maximum of about three to five pixels.

served at ultraviolet wavelengths. The flux profiles were obtained by summing the fluxes of the individual wavelength bins between 177 and 300 nm. The profiles differ in shape and peak intensity. As might be expected, the noon profile has a peak intensity about an order of magnitude greater than that of the dusk profile. Additionally, the noon profile peaks at about 50 km, whereas the dusk profile peaks at about 70 km and exhibits a much sharper peak.

A modeling analysis of these profiles will yield quantitative information about atmospheric densities and processes. The nitric oxide emissions, in particular, can provide information about the densities of nitrogen and oxygen in the upper atmosphere.[20,21] The nitrogen and oxygen emissions can reveal the energy and energy spectrum of the precipitating electrons that stimulate the emissions.[22] Future research efforts at APL will include the development and use of models to glean such information from the data.

STELLAR OBSERVATIONS

The U2 instrument observed several discrete stellar sources, and this section discusses observations of the ultraviolet star Mimosa (Beta Crucis). A type B0.5 III star, Mimosa emits strongly in the ultraviolet region and has an absolute visual magnitude of 1.26 and an ultraviolet-blue magnitude of -1.00.[23] The star varies about 0.06 in magnitude in 5.675 h. Mimosa was chosen as a calibration star because of its strong emissions in the ultraviolet region. During the U2 observations of Mimosa, the spectrographs operated in a gimbal scanning mode in which their fields of view scanned across the location of the star, first sampling the sky background and then the star itself.

Figure 9 is an enlargement of the visible camera's picture of Mimosa. Each pixel has an angular dimension of $6.25° \times 10^{-3}$ on a side, or 3.91×10^{-5} deg^2. The actual star occupies a position within the brightest one or two pixels of the scene. The combined effects of optical focusing and CCD pixel spreading smear out the image of the star. A measure of this spreading is the full width at half maximum, which is about three pixels, although the effect extends farther. The star image actually reaches background beyond about five pixels from the brightest central pixel, so the star's entire image might be considered as large as 10 pixels wide.

Figure 10 shows the spectrum of Mimosa. The star has an essentially continuous spectrum with several prominent features. In the visible region, one can recognize possible helium emissions near 440 nm. (The discontinuities at 310 and 180 nm may be due to intercalibration problems of the spectrographs.) The dotted line below the solid curve indicates the spectrum expected from Mimosa on the basis of previous observations and blackbody calculations. In general, the observed spectrum lies higher in intensity than the expected spectrum; the differences are most pronounced in the mid-ultraviolet region.

Observations of the other calibration stars did not generally show such great differences between the expected and observed spectra, although the observed intensities were generally 3 to 4 times greater than those expected from the known spectra of the stars. These comparisons indicate that further calibration of the spectrographs is necessary to realize absolute photometric accuracy.

LUNAR OBSERVATIONS

The U2 instrument observed the Moon near its last quarter, about 7 days after the full Moon. As the stellar observations measured the instrument response to a point source, the lunar observations measured the in-

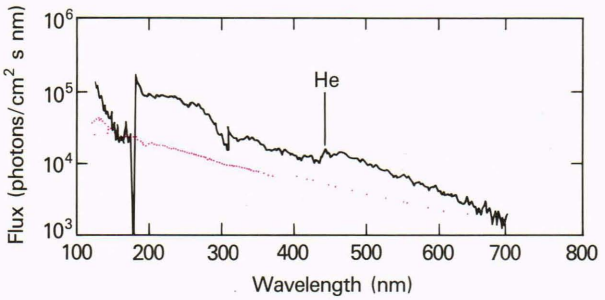

Figure 10—Mimosa spectrum (solid line) compared with the expected spectrum (dotted line) constructed from observations and blackbody estimates.

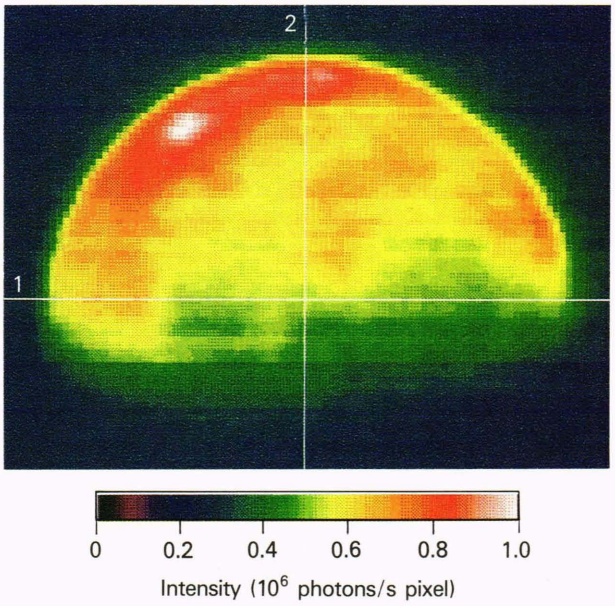

Figure 11—The Moon as viewed by the visible imager. Intensity cuts along lines 1 and 2 appear in Fig. 12.

strument response to an extended source having sharp (i.e., airless) edges.

Figure 11 shows the Moon as seen by the visible imager. The Sun is toward the top, and the Moon's northern pole is toward the right. Various surface features such as lunar maria cause much of the color variation apparent in each frame.

One can construct an edge curve (i.e., a type of extinction curve) of pixel intensity value versus pixel number to determine how sharply the imagers can measure the limb of the Moon, which has an extremely clean edge. Intensity cuts were made along lines 1 and 2 in Fig. 11 to generate the edge curves shown in Fig. 12. Line 1 is approximately parallel to the terminator line, and line 2 is approximately perpendicular to the terminator line. In both cases, the curves exhibit some variations because of surface features; surface features usually affect the perpendicular profile more than the parallel profile and preclude the use of the standard full width at half maximum measure.

The parallel profile in Fig. 12 exhibits the sharpest drop-offs. The parallel edge-curve intensities decrease by

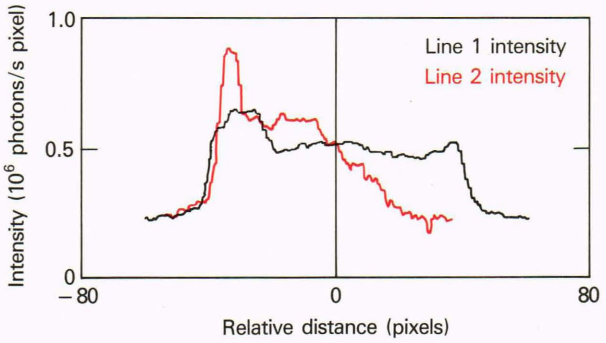

Figure 12—Edge curves from the visible image of the Moon shown in Fig. 11. Line 1 is parallel to the terminator, and line 2 is perpendicular to the terminator.

about a factor of 2 in five pixels. After the region of steepest descent, these edge curves decrease by an additional small percentage in about 10 to 15 pixels. Therefore, the sharpest edges occupy at least five pixels, whereas the decline to actual scene background may require another 10 pixels.

The perpendicular edge in Fig. 12 is much less sharply defined than the parallel edges because of surface features, Earth shine, and the oblique angle at which the sunlight strikes the near-terminator surfaces. The perpendicular curve crossing the terminator line requires about 35 pixels to fall to the background level. The intensity drop-off appears to be linear and does not exhibit the expected cosine dependence. The rate of decrease is significantly slower than that for the parallel curves. Thus, analysis of the stellar point source and the lunar edge source indicates that the imagers have a pixel spreading of three to five pixels for even the most sharply defined points and edges.

CONCLUSIONS

The U2 instrument used small optical detectors to observe various backgrounds of interest to aeronomy and astronomy. The observations provided an internally consistent set of measurements of the noon, midnight, dawn, and dusk limbs of the Earth; of the Moon; and of certain stars. Such measurements will prove valuable to the aeronomy community because they encompass both altitudinal and local time variations of the terrestrial airglow. The measurements will also find application in the space science community in general because they define the ultraviolet and visible backgrounds encountered by an orbital station. Finally, edge and point analyses of the images establish the limits of the electro-optical sensors employed in the measurements.

REFERENCES

[1] D. M. Packer, "Altitudes of the Night Airglow Radiation," *Ann. Geophys.* **17**, 67 (1961).
[2] W. G. Fastie, H. M. Crosswhite, and T. P. Markham, "Far Ultraviolet Auroral Spectra with a Rocket Ebert Spectrometer," *Ann. Geophys.* **17**, 109, (1961).
[3] H. M. Crosswhite, E. C. Zipf, Jr., and W. G. Fastie, "Far Ultraviolet Auroral Spectra," *J. Opt. Soc. Am.* **52**, 643 (1962).
[4] C. A. Barth, "Rocket Measurements of the Nitric Oxide Dayglow," *J. Geophys. Res.* **69**, 3301 (1064).

[5] C. A. Barth and S. Schaffner, "OGO-4 Spectrometer Measurements of the Tropical Ultraviolet Airglow," *J. Geophys. Res.* **75**, 4299 (1970).
[6] T. A. Chubb and G. T. Hicks, "Observations of the Aurora in the Far Ultraviolet Airglow," *J. Geophys. Res.* **75**, 1290 (1970).
[7] E. I. Reed and S. Chandra, "The Global Characteristics of Atmospheric Emissions in the Lower Thermosphere and Their Aeronomic Implications," *J. Geophys. Res.* **80**, 3053 (1975).
[8] C. D. Anger, W. Sawchuck, and G. G. Shepherd, "Polar Cap Optical Aurora Seen from ISIS-2," in *Magnetospheric Physics*, B. M. McCormac, ed., D. Reidel, Hingham, Mass. (1974).
[9] S. Chandra, E. I. Reed, R. R. Meier, C. B. Opal, and G. T. Hicks, "Remote Sensing of the Ionospheric F Layer by Use of OI 6300 Å and OI 1356 Å Observations," *J. Geophys. Res.* **80**, 2327 (1975).
[10] R. S. Stolarski and M. R. Schoeberl, "Further Interpretation of Satellite Measurements of Antarctic Total Ozone," *Geophys. Res. Lett.* **13**, 1210 (1986).
[11] M. R. Schoeberl, A. J. Krueger, and P. A. Newman, "The Morphology of the Antarctic Total Ozone as Seen by TOMS," *Geophys. Res. Lett.* **13**, 1217 (1986).
[12] A. J. Krueger, M. R. Schoeberl, and R. S. Stolarski, "TOMS Observations of Total Ozone in the 1986 Antarctic Spring," *Geophys. Res. Lett.* **14**, 527 (1987).
[13] L. A. Frank, J. D. Craven, and R. L. Rairden, "Images of the Earth's Aurora and Geocorona from the Dynamics Explorer Mission," *Adv. Space Res.* **5**, 53 (1985).
[14] L. A. Frank, J. D. Craven, D. A. Gurnett, S. D. Shawhan, D. R. Weimer, J. L. Burch, J. D. Winningham, C. R. Chappell, J. H. Waite, R. A. Heelis, N. C. Maynard, M. Suguira, W. K. Peterson, and E. G. Shelley, "The Theta Aurora," *J. Geophys. Res.* **91**, 3177 (1986).
[15] S. B. Mende, P. M. Banks, R. Nobles, O. K. Garriott, and J. Hoffman, "Photographic Observations of Earth's Airglow from Space," *Geophys. Res. Lett.* **10**, 1108 (1983).
[16] M. R. Torr and D. G. Torr, "Atmospheric Spectral Imaging," *Science* **225**, 169 (1984).
[17] R. E. Huffman and C.-I. Meng, "Ultraviolet Imaging of Sunlit Auroras from HILAT," *Johns Hopkins APL Tech. Dig.* **5**, 138 (1984).
[18] C.-I. Meng and R. E. Huffman, "Ultraviolet Imaging from Space of the Aurora under Full Sunlight," *Geophys. Res. Lett.* **11**, 315 (1984).
[19] C.-I. Meng and R. E. Huffman, "Preliminary Observations from the Auroral and Ionospheric Remote Sensing Imager," *Johns Hopkins APL Tech. Dig.* **8**, 303 (1987).
[20] P. D. Feldman and P. Z. Takacs, "Nitric Oxide Gamma and Delta Band Emission at Twilight," *Geophys. Res. Lett.* **1**, 169 (1974).
[21] R. P. McCoy, "Thermospheric Odd Nitrogen, 1. NO, N(^{4}S), and O(^{3}P) Densities from Rocket Measurements of the NO Delta and Gamma Bands and the O_2 Herzberg I Bands," *J. Geophys. Res.* **88**, 3197 (1983).
[22] R. R. Meier, R. R. Conway, P. D. Feldman, D. J. Strickland, and E. P. Gentieu, "Analysis of Nitrogen and Oxygen for Ultraviolet Auroral Emissions," *J. Geophys. Res.* **87**, 2444 (1982).
[23] *The Astronomical Almanac for the Year 1987*, U.S. Government Printing Office, Washington, D.C. (1987).

ACKNOWLEDGMENTS—The authors wish to express their gratitude to B. Joy Hook and Eric C. King for their enthusiastic support in programming the microVAX computer and Perceptics image processor on which the data were displayed and analyzed.

THE AUTHORS

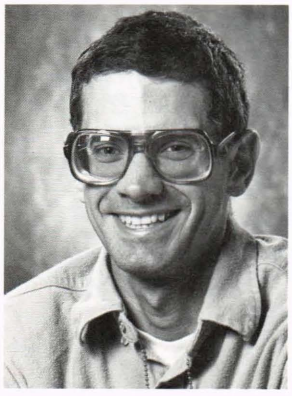

JAMES F. CARBARY was born in Corry, Pa., in 1951 and grew up in Cook County, Ill. He obtained a B.S. in physics from the University of Illinois in 1973 and M.S. and Ph.D. degrees in space physics from Rice University in 1977. He came to APL in 1978 as a postdoctoral research associate, where he analyzed data from the Low Energy Charged Particle experiment on Voyagers 1 and 2. From 1983 to 1985, Dr. Carbary worked at Mission Research Corp. in Albuquerque, where he simulated the electromagnetic pulse effects from nuclear detonations. He rejoined APL in 1985 and, in conjunction with auroral and airglow phenomena, has analyzed particle and optical data from the DMSP, HILAT, and Polar BEAR satellites. Most recently, he served as assistant program scientist for the Delta 180 and 181 missions.

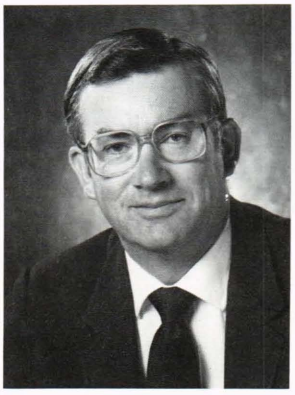

GLEN H. FOUNTAIN is the program manager of the Hopkins Ultraviolet Telescope at APL and Supervisor of the Space Science Instrumentation Group in APL's Space Department. He received his B.S. and M.S. degrees in electrical engineering from Kansas State University in 1965 and 1966, and then joined APL in 1966 as a member of the Attitude Control Group.

During his tenure in the Attitude Control Group, Mr. Fountain helped to develop the attitude control systems for the Small Astronomy Satellites and the TRIAD and TIP satellites. He was appointed assistant program scientist for the MAGSAT satellite in 1976. In that position, he was responsible for the attitude determination system and the hardware development of the attitude control system. He assumed the role of program manager for the Hopkins Ultraviolet Telescope at APL in 1979. Mr. Fountain was appointed Supervisor of the newly formed Space Science Instrumentation Group in 1982. In that position, he is involved in the planning of new instrument designs and in directing their development.

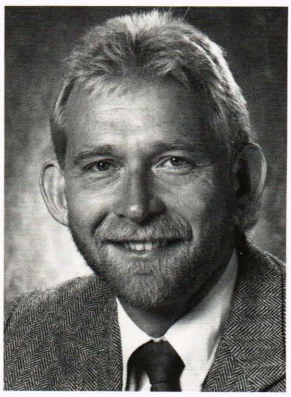

JOHN S. HANSEN is a member of the Computer Science and Technology Group in APL's Space Department. He received B.A. degrees (mathematics and physics, 1971) from the University of Utah, an M.S. degree (computer science, 1988) from The Johns Hopkins University, and a Ph.D. (physics, 1975) from the University of Durham, Durham, England. Before coming to APL, Dr. Hansen investigated the electromagnetic interaction of high-energy (>1 TeV) cosmic-ray muons for the University of Durham, extremely-high-energy ($\sim 10^{19}$ eV) cosmic-ray extensive air showers for the University of Nottingham, and extragalactic neutrinos for the University of California, Irvine.

In 1978, Dr. Hansen joined APL's Submarine Technology Magnetics Group, where he has worked in instrumentation engineering, data analysis, and signal processing. In 1985, he established the Bioelectromagnetics Laboratory. Since 1986, he has been in the Space Department, where he has worked on the Delta 181 project, first as the lead engineer for the U2 spectrographs and later as the Delta 181 data manager.

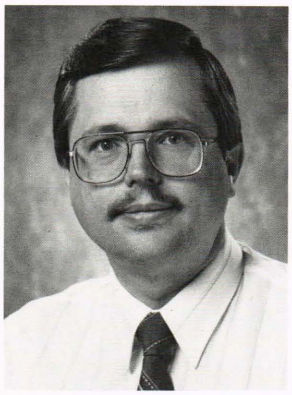

DENNIS E. FORT was born in Winston-Salem, N.C., in 1948. He graduated from North Carolina State University, where he received B.S. and M.E.E. degrees in electrical engineering in 1971 and 1972, respectively. In 1973 he joined APL's Space Physics Group, where he was involved in the development of the Low Energy Charged Particle experiment for the Voyager spacecraft. He subsequently developed instrumentation for the IUE, Galileo, and AMPTE spacecraft and was the system engineer for the particle experiment on the Ulysses spacecraft. More recently, he was the lead engineer in the development of several spaceborne intensified imagers operating in the visible and ultraviolet portions of the spectrum. He is now a Section Supervisor in the Information Processing Group in the Submarine Technology Department.

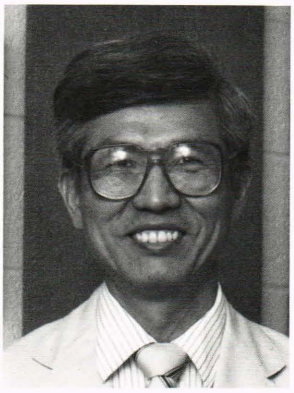

CHING-I. MENG was born in Sian, China, in 1940 and grew up in Taiwan. He came to the Geophysical Institute of the University of Alaska in 1963 to study polar geophysical phenomena based on data collected during the International Geophysical Year. From 1969 to 1978, he was a research physicist at the Space Sciences Laboratory at the University of California, Berkeley, where he specialized in the morphology of magnetospheric physics. Dr. Meng joined APL in 1978. His research involves solar–terrestrial interactions, plasma and field morphology of the magnetosphere, spacecraft charging, and the emissions of the terrestrial atmosphere. He also investigates the global imaging of aurora and airglow. Dr. Meng recently served as the program scientist for the Delta 180 and 181 missions.